Supporting Information

In-situ rapid formation of a nickel-iron based electrocatalyst for water oxidation

Jianying Wang, Lvlv Ji, and Zuofeng Chen*

Shanghai Key Lab of Chemical Assessment and Sustainability, School of Chemical Science and Engineering, Tongji University, Shanghai 200092, China

*E-mail: zfchen@tongji.edu.cn

EXPERIMENTAL

Chemicals. Nickel(II) nitrate ($Ni(NO_3)_2 \cdot 6H_2O$, 98%), iron(III) sulfate ($Fe_2(SO_4)_3$, 99%), iron(II) sulfate ($FeSO_4 \cdot 7H_2O$, 99%), sodium carbonate (Na_2CO_3, > 99.8%), sodium bicarbonate ($NaHCO_3$, 100.3%), and potasium hydroxide (KOH, 99%) were obtained from Fisher Scientific. Indium tin oxide (ITO) glass (11 Ω sq^{-1}) was obtained from Delta Technologies, Limited. Nickel foam (NF, thickness ~ 0.5 mm, bulk density ~ 0.56 g/cm^3) was obtained from Shanxi Lizhiyuan Material of Battery Co. Ltd (China). All other reagents were analytical grade and used as received. All electrolyte solutions were prepared by Milli-Q ultrapure water (> 18 MΩ) unless stated otherwise. The concentrated Na_2CO_3 solution of pH 10.8 is prepared by mixing Na_2CO_3 and $NaHCO_3$ ($c(CO_3^{2-}) + c(HCO_3^-)$ = 2 M). The pH for 1 M KOH is 13.6 according to literature reports.[1,2]

Apparatus. UV-visible spectroscopy was recorded on a SPECORD$^®$ 200 PLUS (analytikjena, Germany) diode-array spectrophotometer. A blank ITO was used as reference during the measurement. The average transmittance in wavelength between 400 - 900 nm was

used to evaluate the transparency of the catalyst film. The decrease in transmittance is assumed to be proportional to the thickness of the catalyst film which is used to calculate the thickness of the catalyst film by 15-min and 30-min CPE by referring the thickness of the catalyst film by 60-min CPE determined by AFM measurement.

Scanning electron microscope (SEM) images, energy dispersive X-ray analysis (EDX) data and EDX mapping images were obtained at Hitachi S-4800 (Hitachi, Japan) equipped with a Horiba EDX system (X-max, silicon drift X-Ray detector). SEM Images were obtained with an acceleration voltage of 3 kV and EDX mapping images and EDX spectra were obtained with acceleration voltages between 15 kV. The time for EDX mapping images is 15 min. After electrodeposition from CPE, the catalyst-coated electrode was rinsed with deionized water and dried in air before being loaded into the instrument.

Transmission electron microscopy (TEM) images, high resolution TEM (HRTEM) images and selected area electron diffraction (SAED) pattern were obtained using JEM-2100, JEOL. The $NiFeO_x$/ITO slides were rinsed gently with deionized water and dried in air. The $NiFeO_x$ catalyst was scraped from the ITO electrode substrate and dispersed in the absolute ethanol uniformly, and a drop of the mixture was dried on a carbon-coated copper grid for analysis.

The catalyst film on the ITO and nickel foam was imaged through a bright field optical microscope (Olympus BX51) fitted with a Olympus DP27 camera. The magnification is 200 (20×10) or 1000 (100×10) times the original size.

Because the catalyst film is very thin, the cross-sectional SEM images could not clearly dispaly the boundary between the catalyst film and the ITO substrate. Therefore, the thickness of the catalyst film was determined by an Atomic Force Microscope (AFM, CSPM-4000). The $NiFeO_x$/ITO electrode was immobilized on the platform by a double side tape. Contact-mode AFM was ultilized to scan the sample in air at room temperature. Processing and analysis of the images were carried out using CSPM 4.5 image software.

Powder X-ray diffraction (XRD) was measured by Bruker Foucs D8 via ceramic monochromatized Cu Kα radiation of 1.54178 Å, operating at 40 kV and 40 mA. The scanning rate was 5° per min in 2θ and the scanning range was from 10 - 80°.

X-ray photoelectron spectroscopy (XPS) for elemental analysis was conducted on a Kratos Axis Ultra DLD X-ray Photoelectron Spectrometer using 60 W monochromated Mg Kα radiation as the X-ray source for excitation. The 500 μm X-ray spot was used for XPS analysis. The base pressure in the analysis chamber was about 3×10^{-10} mbar. The carbon 1s peak (284.6 eV) was used for internal calibration. The peak resolution and fitting were processed by XPS Peak 41 software.

The nickel and iron coverage of catalyst film by 15-min CPE with 1 mM Ni(II) and 1 mM Fe(III) was determined by the ICP-OES using the Perkin Elmer ICP-OES Optima 8300. The sample of the $NiFeO_x$ film formed by 15-min CPE on 0.5 cm^2 ITO was dissolved in 2.5 mL of 0.1 M HNO_3. The iron and nickel concentration of 0.201 mg/L and 0.234 mg/L was obtained using the working curve method, respectively, which suggested that 18 nmol of iron and 20 nmol of nickel were electrodeposited onto ITO electrode per square centimeter. This result corresponded to 27 iron atoms and 30 nickel atoms per 25 Å^2. This number indicates the formation of a 11-atom-layer film in 15-min CPE. Similarly, the ICP-OES measurement revealed a 7-atom-layer for the optimized catalyst film by 3-min CPE with 0.6 mM Ni(II) and 1.4 mM Fe(III).

Electrochemical measurements were performed on a CHI 660E electrochemical workstation (Chenhua Corp., Shanghai, China). The three-electrode system consisted of a working electrode, a platinum plate counter electrode, and a saturated calomel reference electrode (SCE, ~0.244 V *vs.* NHE). Prior to each measurement, the platinum plate counter electrode was routinely treated by soaking in 1 M hydrochloric acid to remove any deposited Ni or Fe. Unless stated otherwise, all potentials in cyclic voltammetry and controlled potential

electrolysis were reported *vs.* NHE without *iR* compensation. All experiments were performed at 22 ± 2 °C.

Procedure. *Electrode pretreatment and preparation.* Prior to electrochemical measurements, ITO glass electrodes were cleaned by sonication in pure water (15 min), isopropanol (15 min), and acetone (15 min), respectively. Nickel foam was sonicated in 5 M HCl solution for 10 min to remove the NiO_x layer on the surface, which was subsequently rinsed with deionized water and dipped in 2 M Na_2CO_3 solution for 2 minutes, then rinsed with deionized water again and dried in the air at 50 °C.

The active catalyst film was developed *in-situ* on the ITO electrode or nickel foam electrode by electrolysis in 2 M Na_2CO_3 (pH 10.8) containing 1 mM Ni(II) & 1 mM Fe(II or III) at 1.30 V for various time. The saturation of the current density after 15 min (with Ni(II) & Fe(III)) or 3 min (with Ni(II) & Fe(II)) indicates that the electrode substrate is largely covered by the precipitated catalyst film.

Fe(II) as a precursor component. Fe(II) stock solution was prepared with deaerated water immediately before use. The electrolyte solution was vigorously bubbled with nitrogen gas for at least 30 min to remove oxygen in the solution before the dissolution of FeSO4 and a constant flow of N_2 was maintained over the electrolyte solution during the measurements.

Calculation of ECSA. The electrochemically active surface area (ECSA) of the electrocatalysts is evaluated by measurement of their double layer charging capacitance in 1 M KOH solution. Briefly, a potential range where no apparent Faradaic process occurred was determined firstly using the cyclic voltammetry (CV). The charging current (i_c) in this potential range was then measured from CVs at different scan rates. The relation between i_c, the scan rate (v), and the double layer charging capacitance (C_{DL}) was governed by eq 1. The ECSA, which is directly proportional to C_{DL}, can be evaluated from the slope of the plot of i_c *vs.* v.

$$i_c = vC_{DL} \qquad (1)$$

Tafel plot. The current-potential data of an ITO or nickel foam with an active $NiFeO_x$ catalyst coating were obtained by linear sweep voltammetry (LSV) at a very slow scan rate (0.1 mV/s). The Tafel slope was obtained from the LSV plot using a linear fit applied to points in the Tafel region. The solution resistance measured prior to the data collection (using *iR* test function) was used to correct the Tafel plot for *iR* drop.

TOF calculation. The TOF is calculated by assuming that all current is used to produce molecular oxygen with 100% Faraday efficiency.

$$TOF = \frac{\text{number of theoretic oxygen molecules}}{\text{total number of nickel and iron atoms in the thin film}}$$

Thin layer film modeling. From the ICP-OES measurement, we obtained 27 Fe atoms and 30 Ni atoms per 25 $Å^2$ by 15-min CPE with Ni(II) & Fe(III). The monolayer coverage was approximated as a surface density of 5 Ni atoms⁄25 $Å^2$ according to literature[3] and we assumed that Fe posseses the same surface density of monolayer coverage (r_{Fe} = 124.1 pm ≈ r_{Ni} = 124.6 pm). Therefore, the formation of a 11-atom-layer film ((27 + 30) / 5 ≈ 11) by 15-min CPE with Ni(II) & Fe(III) could be achieved. Similarly, the formation of a 7-atom-layer film by 3-min CPE with Ni(II) & Fe(II) could be achieved.
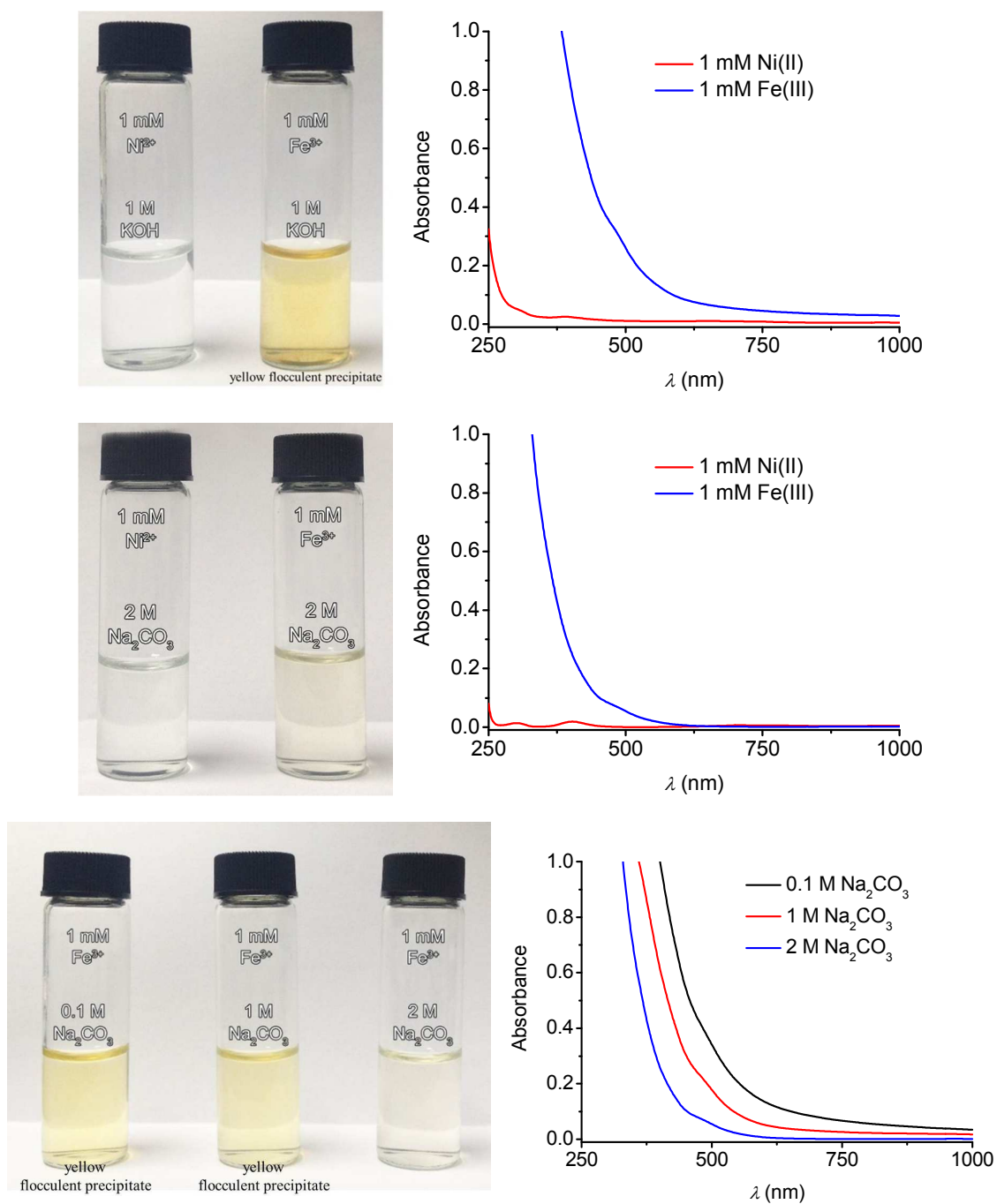
Figure S1. Camera pictures showing the solubility of Ni(II) and Fe(III) in solutions of 1 M KOH (pH 13.6), 2 M Na_2CO_3 (pH 10.8), and different concentration of Na_2CO_3 (pH 10.8). In the corresponding UV-Vis spectra, the poor solubility is indicated by the elevated baseline due to the light scattering by the suspended precipitated nanoparticles/nanoclusters. From

these Figures, it can be seen that Fe(III) is insoluble in 1 M KOH (pH 13.6), insoluble in Na$_2$CO$_3$ (pH 10.8) of $\leq$ 1 M, but soluble in 2 M Na$_2$CO$_3$ (pH 10.8).
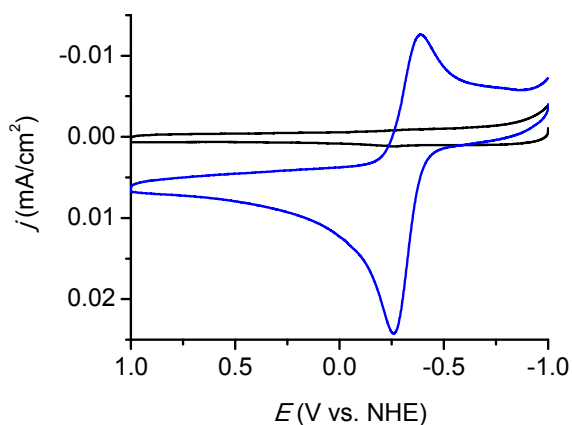
Figure S2. CVs at an ITO electrode without (black) and with (blue) addition of 2 mM Fe(II) in 2 M Na$_2$CO$_3$ (pH 10.8) showing the redox potential of Fe(III/II) in concentrated carbonate. Scan rate, 100 mV/s. Similar CV profile was obtained with addition of 2 mM Fe(III) in 2 M Na$_2$CO$_3$ (pH 10.8).
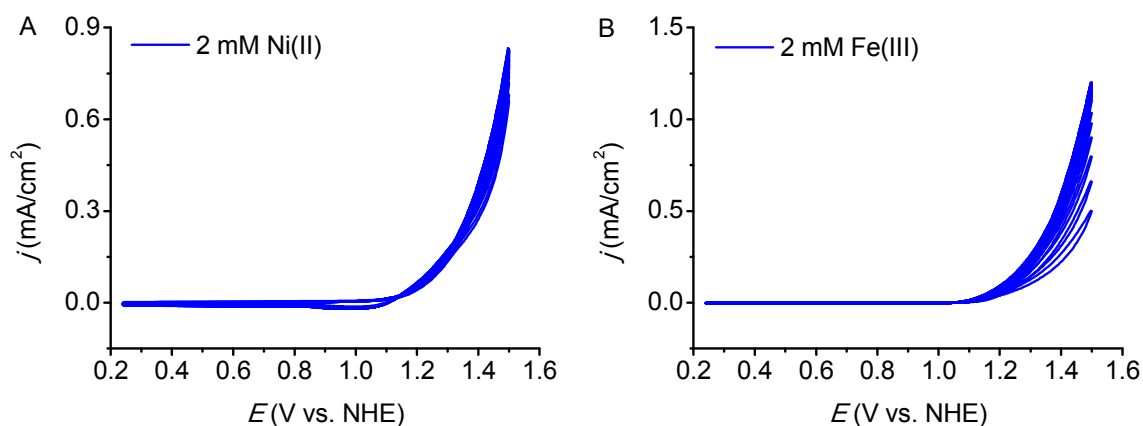
Figure S3. (A) Successive CVs (25 scan cycles) of an ITO electrode in 2 M Na$_2$CO$_3$ (pH 10.8) containing 2 mM Ni(II). (B) As in (A) with 2 mM Fe(III). Scan rate, 100 mV/s.
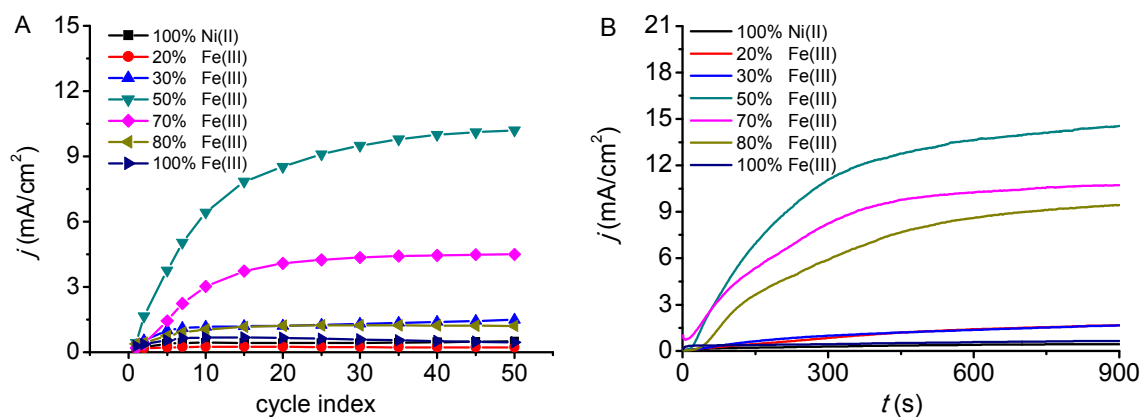
Figure S4. (A) Dependence of the current density at 1.3 V on the scan cycle. (B) Controlled potential electrolyses at 1.3 V with varied molar ratio of Ni(II):Fe(III).
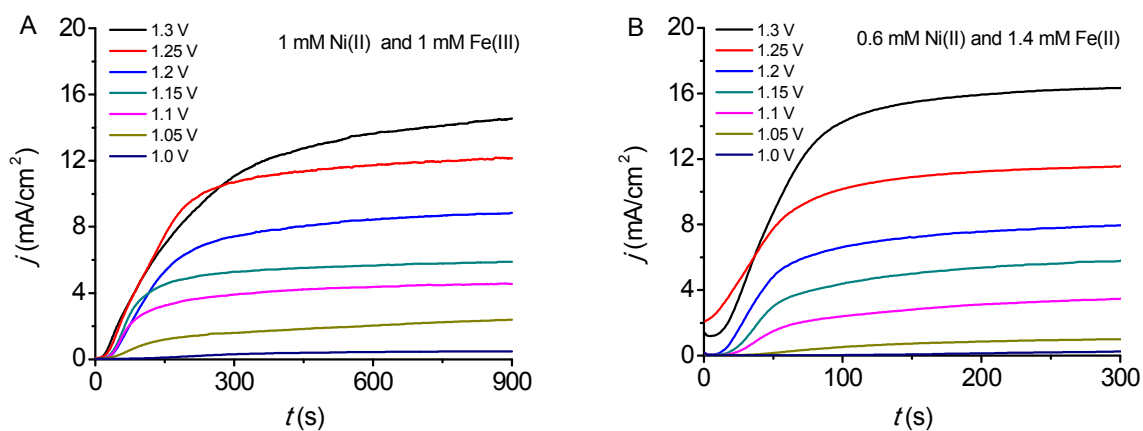
Figure S5. (A) Controlled potential electrolyses at various potentials with 1 mM Ni(II) & 1 mM Fe(III) in 1 M KOH. (B) As in (A), with 0.6 mM Ni(II) & 1.4 mM Fe(II). Electrode, ITO.
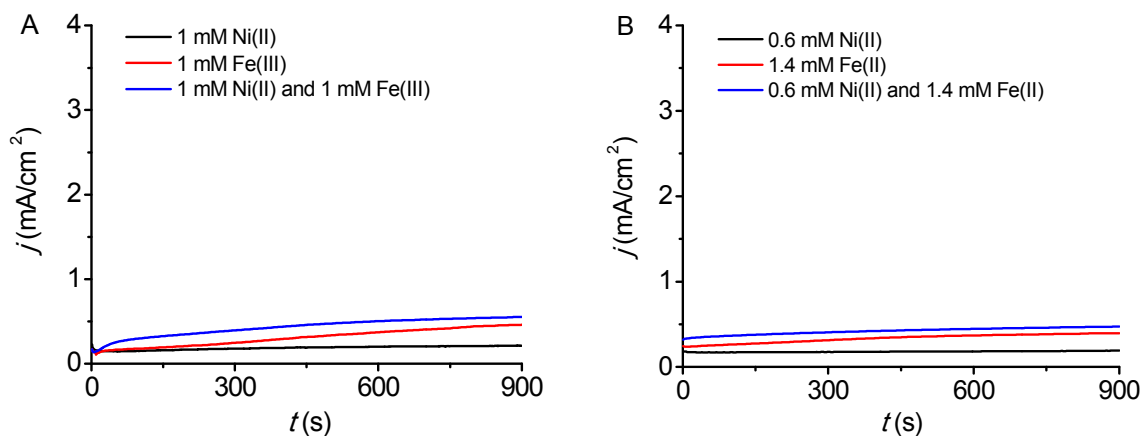
Figure S6. (A) Controlled potential electrolyses at 1 V with 1 mM Ni(II), 1 mM Fe(III), or 1 mM Ni(II) & 1 mM Fe(III) in 1 M KOH. (B) As in (A), with 0.6 mM Ni(II), 1.4 mM Fe(II), or 0.6 mM Ni(II) & 1.4 mM Fe(II). Electrode, ITO.
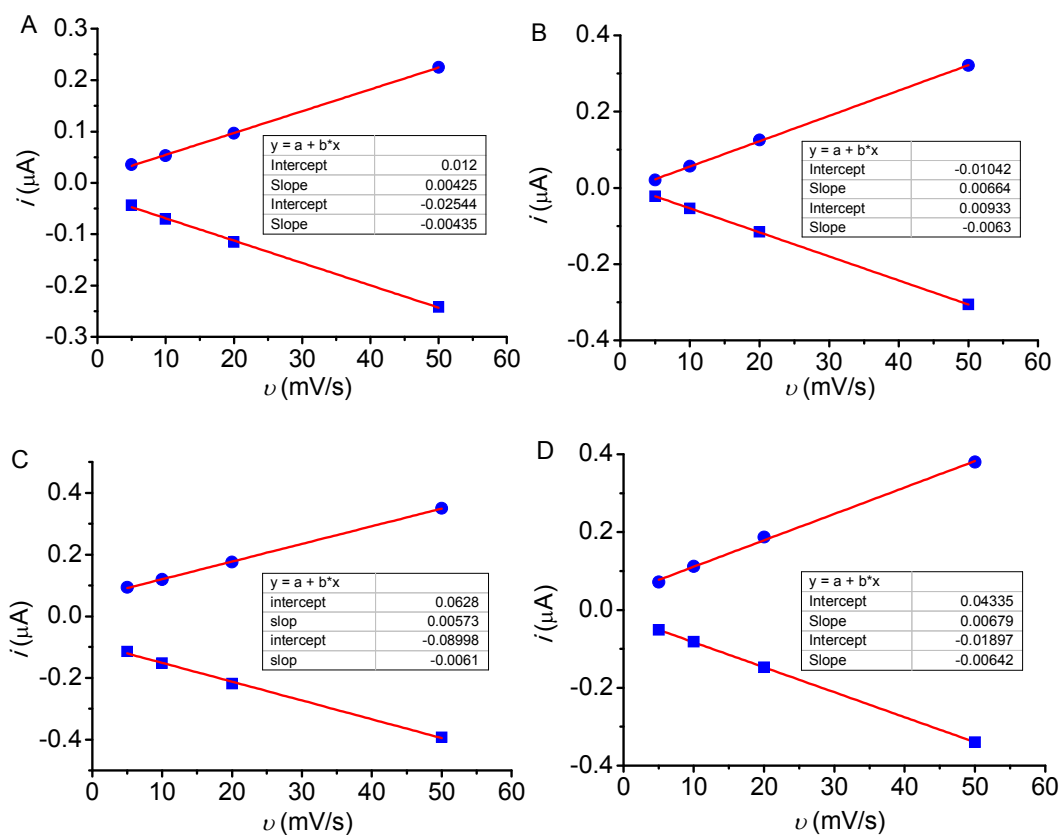
Figure S7. Double layer charging capacitance measurements for determination of the electrochemically active surface area of a NiFeO$_x$ catalyst film on the ITO electrode from CVs in 1 M KOH. (A) blank ITO electrode, (B) 15-min CPE, (C) 30-min CPE, (D) 60-min CPE.
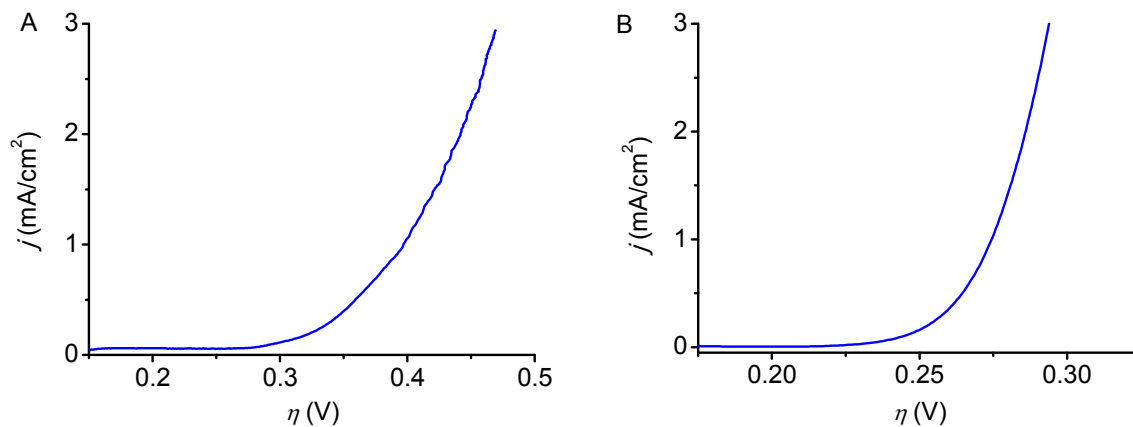

Figure S8. LSVs of the as-prepared catalyst film in different solution, (A) 2 M Na$_2$CO$_3$, (B) 1 M KOH. Scan rate, 0.1 mV/s.
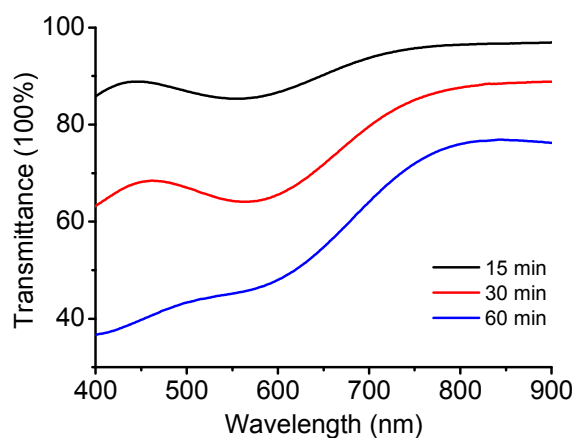

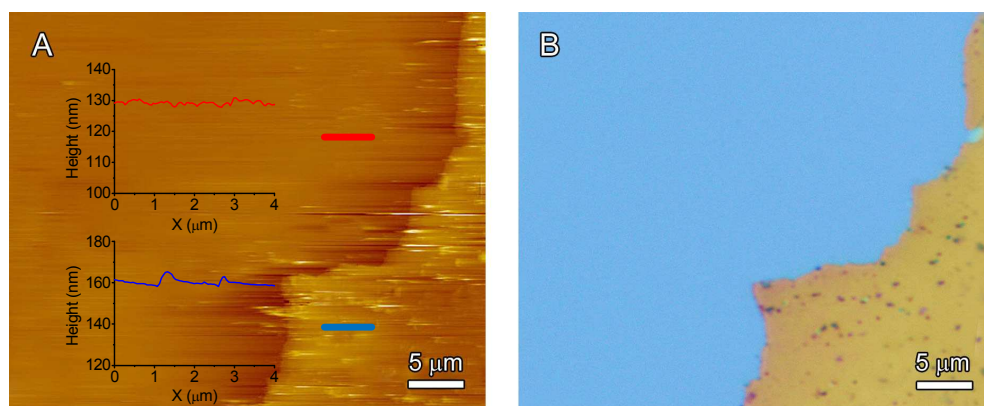**Figure S9.** UV-vis of the different ITO catalyst films.

Figure S10. (A) AFM image showing the boundary of the catalyst film and the ITO substrate with the associated height profile in the inset. (B) Corresponding bright field optical microscopy image. The catalyst film was prepared by 60-min CPE.
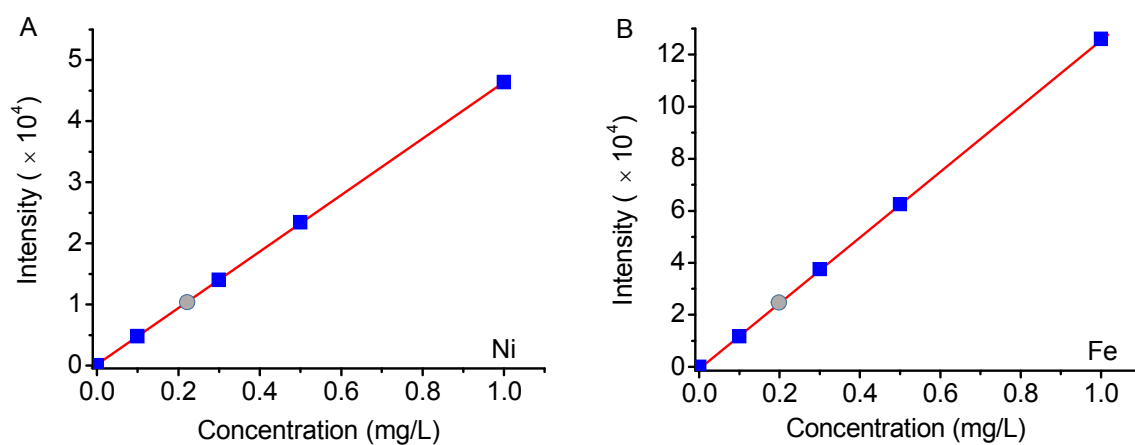

Figure S11. The working curves of Ni (A) and Fe (B) by ICP-OES. The circle symbols indicate the concentration of Ni and Fe in the made-up sample.
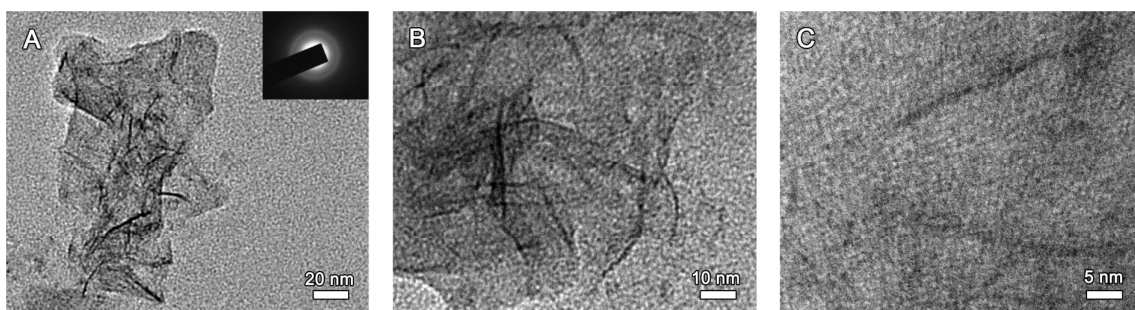
Figure S12. TEM and HRTEM images of a sample of the as-prepared NiFeO$_x$ film scraped from the ITO electrode. The insert in (A) is the selected-area electron diffraction pattern (SAED) of the film.
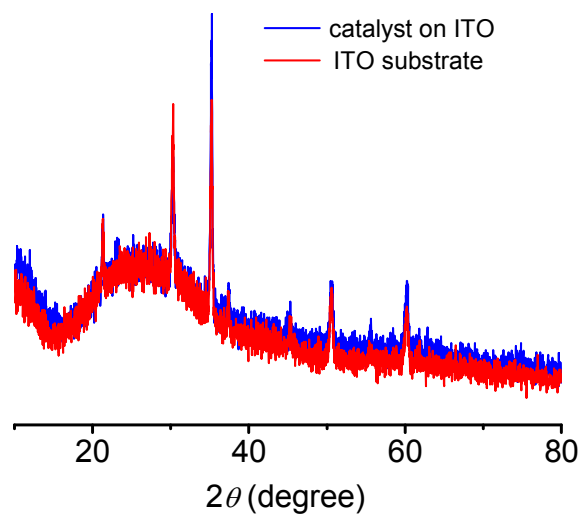

Figure S13. XRD patterns of ITO before and after constant potential electrolysis at 1.3 V *vs*. NHE in 2 M Na$_2$CO$_3$ (pH 10.8) with 1 mM Ni(II) and 1 mM Fe(III).
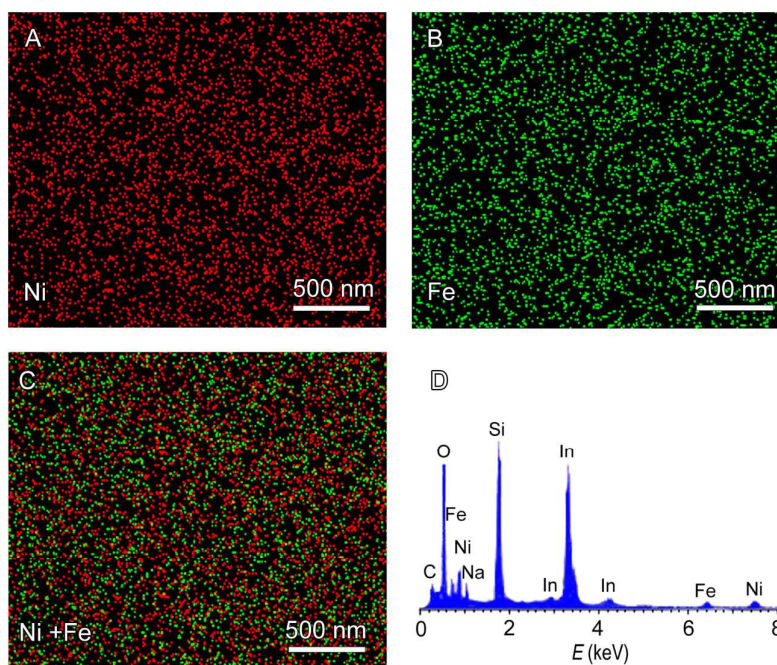
Figure S14. EDX mapping and EDX elemental analysis of the NiFeO$_x$/ITO electrode.
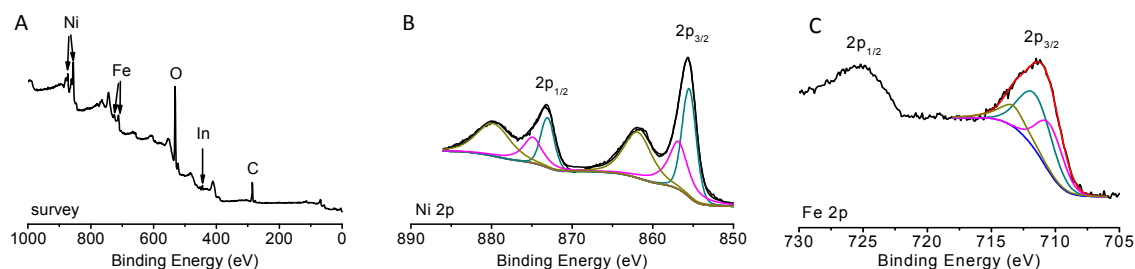

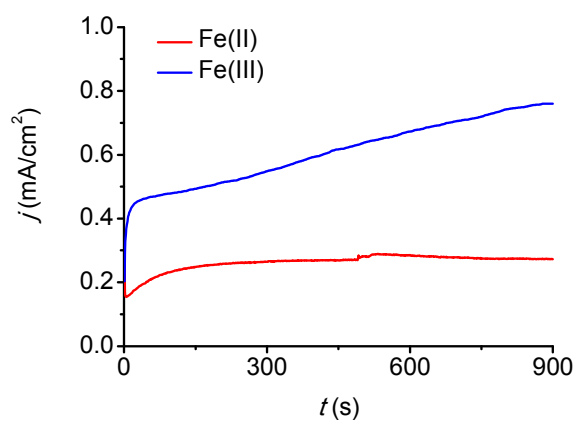**Figure S15.** XPS of the as-prepared NiFeO$_x$ catalyst film.

Figure S16. Controlled potential electrolyses at 1.3 V with individual Fe(II) or Fe(III) in 2 M Na$_2$CO$_3$ (pH 10.8). The curve with Fe(II) is taken from the black line in Figure 4A, and the curve with Fe(III) is tatken from the black line in Figure S4B.
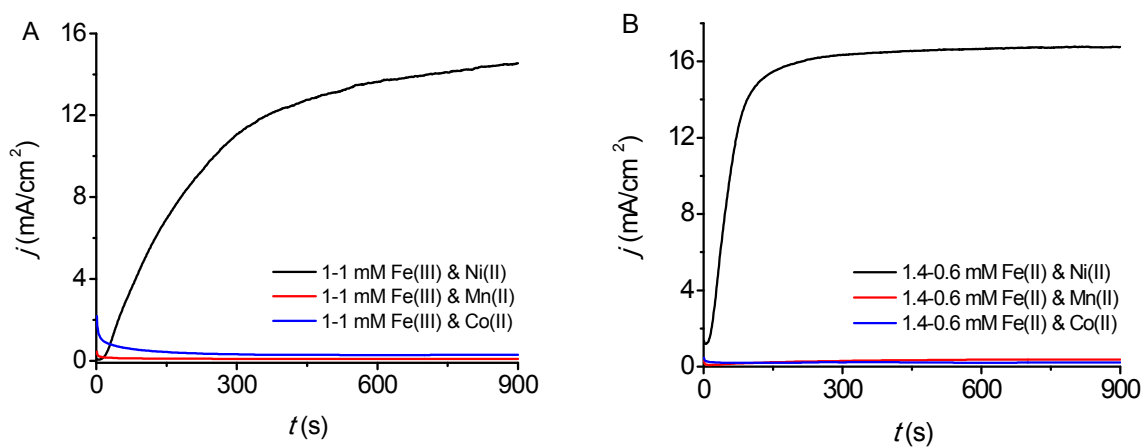
Figure S17. (A) Controlled potential electrolyses at 1.3 V with 1 mM Fe(III) & 1 mM Ni(II) or Mn(II) or Co(II) in 2 M Na_2CO_3 (pH 10.8). (B) Controlled potential electrolyses at 1.3 V with 1.4 mM Fe(II) & 0.6 mM Ni(II) or Mn(II) or Co(II) in 2 M Na_2CO_3 (pH 10.8).
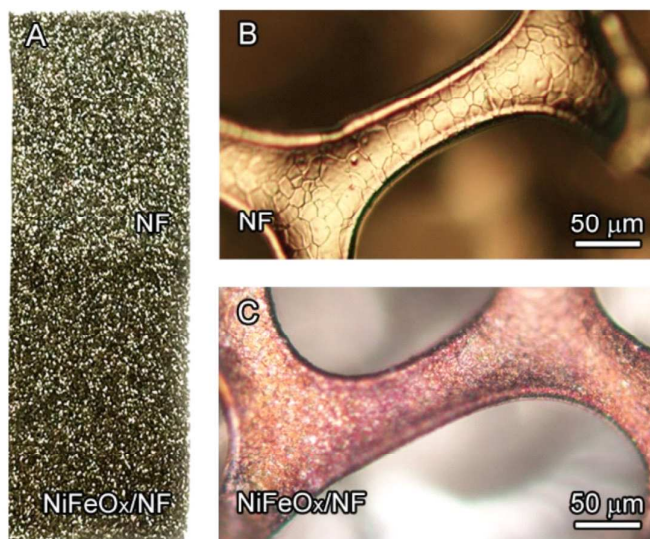

Figure S18. Photograph and dark field optical microscopy of the pure NF electrode and the $NiFeO_x/NF$ electrode.
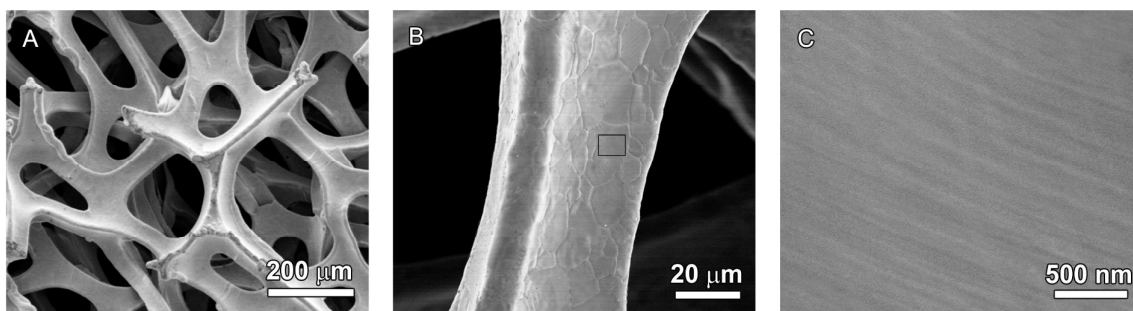
Figure S19. (A,B) SEM images of the pure NF. (C) High-resolution SEM image of the area squared in (B).
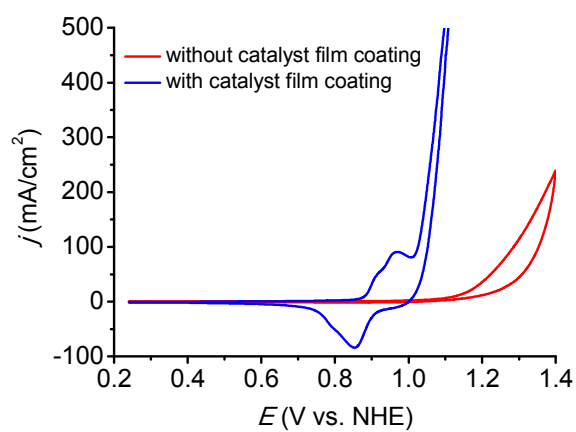

Figure S20. CVs of the nickel foam electrode with and without $NiFeO_x$ catalyst film coating in 2 M Na_2CO_3 (pH 10.8). Scan rate, 100 mV/s.

Table S1. The methods for preparation of $NiFeO_x$ electrocatalysts.

Chemicals/Reagents	Methods	Refs
$Ni(NO_3)_2$, $Fe(NO_3)_3$	Cathodic electrodeposition: -1.2 V for 10 s	4
$Ni(OAc)_2$, $Fe(NO_3)_3$	Cathodic electrodeposition: -1 mA/cm^2 for 600 s	5
$NiSO_4$, $FeSO_4$	Cathodic electrodeposition: -50 $\mu A/cm^2$ for 1125 s	6
$NiSO_4$, $FeSO_4$	Cathodic electrodeposition: -50 mA/cm^2 for 150 s	7
$Ni(NO_3)_2$, $FeCl_2$	Cathodic electrodeposition: -1 mA/cm^2	8
$Ni(SO_4)_2$, $FeSO_4$	Cathodic electrodeposition: -50 $\mu A/cm^2$ for 20 s	9
$Ni(NO_3)_2$, $Fe(NO_3)_3$	Cathodic electrodeposition: -3 mA/cm^2 at -1.5 V for 100 s	10
$Ni(NO_3)_2$, $FeCl_2$	Cathodic electrodeposition: -10 mA/cm^2	11
$NiSO_4$, $FeSO_4$	Cathodic electrodeposition: -0.35 mA/cm^2 for 40 min	12
$Ni(NO_3)_2$, $Fe_2(SO_4)_3$ or $FeSO_4$	Anodic electrodeposition: $+1.05$ to $+1.3$ V for 300-900s	This work

Table S2. Comparison of catalytic performace of the $NiFeO_x$ catalysts at 2D planar substrates.

Materials	Solution	Current density (mA/cm^2)	Overpotential (mV)	Tafel slope (mv/dec)	Refs
Ni-Fe nanotube arrays	0.1M KOH	10	470 mV	105	12
Porous $NiFe_{0.15}O_x$	0.1M KOH	10	328 mV	42	13
$NiFe_{0.12}O_x$ nanocrystals	0.1M KOH	10	300 mV	30	14
$NiFe_{0.4}O_x$	0.1M KOH	5	370 mV	26-44	15
Ni-$Fe_{0.52}$ LDH	1 M KOH	10	330 mV	97	16
NiFe-LDH nanoplates	1 M KOH	10	320 mV	31	5
NiFe-LDH bulk	1 M KOH	10	347 mV	67	17
NiFe-LDH nanosheet	1 M KOH	10	302 mV	40	17
$NiFeO_x$	1 M NaOH	10	350 mV	/	18
$Ni_{0.53}Fe_{0.47}O_x$	1 M KOH	10	310 mV	28	This work

LDH: layered double hydroxide.

References

[1]   Kuai, L.; Geng, J.; Chen, C.; Kan, E.; Liu, Y.; Wang, Q.; Geng, B. *Angew. Chem. Int. Ed. Engl.* **2014**, *53*, 7547-7551.

[2]   Morales-Guio, C. G.; Mayer, M. T.; Yella, A.; Tilley, S. D.; Gratzel, M.; Hu, X. *J. Am. Chem. Soc.* **2015**, *137*, 9927-9936.

[3]   Dinca, M.; Surendranath, Y.; Nocera, D. G. *Proc. Natl. Acad. Sci. USA* **2010**, *107*, 10337-10341.

[4]   Yu, X.; Zhang, M.; Yuan, W.; Shi, G. *J. Mater. Chem. A* **2015**, *3*, 6921-6928.

[5]   Gong, M.; Li, Y.; Wang, H.; Liang, Y.; Wu, J. Z.; Zhou, J.; Wang, J.; Regier, T.; Wei, F.; Dai, H. *J. Am. Chem. Soc.* **2013**, *135*, 8452-8455.

[6]   Louie, M. W.; Bell, A. T. *J. Am. Chem. Soc.* **2013**, *135*, 12329-12337.

[7]   Swierk, J. R.; Klaus, S.; Trotochaud, L.; Bell, A. T.; Tilley, T. D.; *J. Phys. Chem. C* **2015**, *119*, 19022-19029.

[8]   Zou, S.; Burke, M. S.; Kast, M. G.; Fan, J.; Danilovic, N.; Boettcher, S. W. *Chem. Mater.* **2015**, *27*, 8011-8020.

[9]   Friebel, D.; Louie, M. W.; Bajdich, M.; Sanwald, K. E.; Cai, Y.; Wise, A. M.; Cheng, M. J.; Sokaras, D.; Weng, T. C.; Alonso-Mori, R.; Davis, R. C.; Bargar, J. R.; Norskov, J. K.; Nilsson, A.; Bell, A. T. *J. Am. Chem. Soc.* **2015**, *137*, 1305-1313.

[10]   Wang, D.; Zhou, J.; Hu, Y.; Yang, J.; Han, N.; Li, Y.; Sham, T.-K. *J. Phys. Chem. C* **2015**, *119*, 19573-19583.

[11]   Batchellor, A. S.; Boettcher, S. W. *ACS Catal.* **2015**, *5*, 6680-6689.

[12]   Zhao, Z.; Wu, H.; He, H.; Xu, X.; Jin, Y. *J. Mater. Chem. A* **2015**, *3*, 7179-7186.

[13]   Qi, J.; Zhang, W.; Xiang, R.; Liu, K.; Wang, H.-Y.; Chen, M.; Han, Y.; Cao, R. *Adv. Sci.* **2015**, *2*, 1500199.

[14]   Bau, J. A.; Luber, E. J.; Buriak, J. M. *ACS Appl. Mater. Interfaces* **2015**, *7*, 19755-19763.

[15]   Smith, R. D.; Prevot, M. S.; Fagan, R. D.; Trudel, S.; Berlinguette, C. P.; *J. Am. Chem. Soc.* **2013**, *135*, 11580-11586.

[16]   Zhou, L. J.; Huang, X.; Chen, H.; Jin, P.; Li, G. D.; Zou, X. *Dalton Trans.* **2015**, *44*, 11592-11600.

[17]   Song, F.; Hu, X. *Nat. Commun.* **2014**, *5*, 4477.

[18]   McCrory, C. C.; Jung, S.; Peters, J. C.; Jaramillo, T. F. *J. Am. Chem. Soc.* **2013**, *135*, 16977-16987.